Nuclear tunneling effects of charge transport in rubrene, tetracene, and pentacene

Guangjun Nan,[1] Xiaodi Yang,[1] Linjun Wang,[1] Zhigang Shuai,[1,2,*] and Yi Zhao[3]

[1]*Key Laboratory of Organic Solids, Beijing National Laboratory for Molecular Sciences (BNLMS), Institute of Chemistry,
Chinese Academy of Sciences, 100190 Beijing, People's Republic of China*
[2]*Department of Chemistry, Tsinghua University, 100084 Beijing, People's Republic of China*
[3]*State Key Laboratory of Physical Chemistry of Solid Surfaces and Department of Chemistry, Xiamen University,
361005 Xiamen, People's Republic of China*

The mechanism of charge transport in organic materials is still controversial from both experimental and theoretical perspectives. At room temperature, molecular deformations interact strongly with the charge carrier both through intermolecular and intramolecular phonons, suggesting a thermally activated hopping mechanism as described by the Marcus electron transfer theory. However, several experimental measurements have indicated that the electronic transport behaves in a "bandlike" manner, as indicated by a decrease in mobility with increasing temperature, in contradiction to the Marcus description. Bandlike first-principles calculations based on the Holstein-Peierls model tend to overestimate the charge mobility by about 2 orders of magnitude. Here, a hopping model is derived that not only quantitatively describes the charge mobility but also explains the observed bandlike behavior. This model uses the quantum version of charge-transfer theory coupled with a random-walk simulation of charge diffusion. The results bridge the gap between the two extreme mechanisms. This first-principles method predicts the room-temperature hole mobilities to be 2.4, 2.0, and 0.67 $cm^2/V\,s$, for rubrene, pentacene, and tetracene, respectively, in good agreement with experiment.

I. INTRODUCTION

Charge transport in organic semiconductors has aroused strong interest in recent years.[1–4] Room-temperature mobility as high as a few tens of $cm^2/V\,s$ for single-organic crystals have been reported. However, the reported mobilities are strongly dependent on sample preparation and measurement techniques (including the device structures).[1] It is important to gain a complete theoretical understanding of the intrinsic mobility in organic materials, independent of sample preparation, charge injection, or interfaces and to eventually predict the mobility from first principles. Theoretically, there have been two extreme models for transport: hopping and bandlike. The former describes the thermally activated hopping of a charge over a barrier, which results in mobility increasing with temperature due to increased thermal activation. The latter describes a delocalized charge undergoing coherent motion, which results in mobility decreasing with temperature due to increased phonon scattering. A Holstein-Peierls model coupled with first-principles calculation successfully demonstrated bandlike transport behaviors.[5–7] However, the calculated charge mobility is about 2 orders of magnitude larger than experimental value for extra pure organic crystals.[7] On the other hand, past work on charge transfer (CT) in complex organic and biosystems has found that the reorganization accompanying CT, both in the molecule and the surroundings, is typically quite large for organic systems. This reorganization therefore plays an important role in determining the CT processes, such as in the description of the Marcus theory.[8] Indeed, several groups have investigated the electron transport by using a Marcus hopping model to successfully describe organic semiconductors.[9–14] For example, in oligothiophenes ($T_n, n=2-8$), it has been shown that the hopping model can quantitatively describe the effects

of both molecular size and crystal packing on the charge mobility.[15] These results not only help to understand the structure-transport relationships at the molecular level but also indicate that the hopping mechanism is a reasonable description of charge transport in these organic materials, at least at room temperature.

However, several recent measurements indicate that the mobility decreases with temperature, which points to a bandlike mechanism of carrier transport.[16–20] For example, in the rubrene single crystals that have recently aroused wide interest, a bandlike transport behavior has been demonstrated from $T=170$ to 300 K.[4,19,20] Similar behavior has also been demonstrated in purified pentacene from 225 to 340 K.[17] Rubrene is derived from tetracene by attaching four phenyls as side groups (see Fig. 1). Based on band-structure calculations and analysis of electronic couplings, da Silva Filho *et al.*[21] attribute the high mobility in rubrene to the presence of optimal pathways, in the rubrene crystal structure, for hopping of the hole through the phenyl side groups. This is in contradiction to a recent Raman spectroscopy study which found that the intermolecular interactions in rubrene are much weaker than those in polyacenes.[22] From both experimental and theoretical perspectives, the underlying transport mechanism in rubrenes and polyacenes remains unclear.

To explain the bandlike temperature dependence of the mobility, Troisi and Orlandi[23–25] argued that the thermal fluctuation in the electron transfer integral t are very large for organic systems. They simulated a one-dimensional (1D) stack of organic molecules and showed that the mobility decreases with temperature because the temperature increases the thermal disorder, which leads to charge localization and a decrease in mobility. This description accounts for the observed temperature dependence without invoking a bandlike model.[25] This effect of thermal fluctuations has been previously ignored due to thermal averaging over the phonon
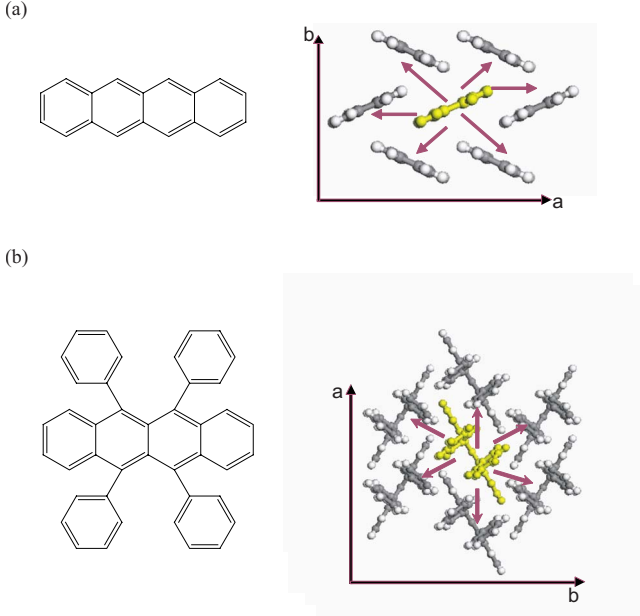
FIG. 1. (Color online) Chemical structures of tetracene and rubrene, along with the most important nearest-neighbor pairs in the crystal structures.

states.[5–7] However, the thermal disorder is known to be much more pronounced for 1D systems, thus the fluctuation amplitude of t was found to be about the same as the value of t itself.[24] For real three-dimensional (3D) materials, such fluctuation should play minor role for charge transport, since first, the thermal fluctuation itself would be much reduced for 3D and even if there is such fluctuation, the charge can make deviation.

In a previous study, based on both the Holstein-Peierls model[7] and the model of Troisi,[25] we indeed found a bandlike temperature dependence in organic materials. But both models required mapping a complex molecular system onto a simple model, with the associated risk of losing important aspects of the actual chemical system. In particular, as pointed out above, the 1D nature of the Troisi model amplifies the thermal fluctuation effects to an unrealistic level. On the other hand, although the Marcus theory has been successfully applied to molecular design,[9–15] it invokes thermal activation and thus fails to give a bandlike description. In this work, we propose a method that couples quantum CT theory with a random-walk simulation. We find that by including the effects of quantum nuclear tunneling, the bandlike temperature dependence can be explained within a hopping model and, at the same time, the approach possesses the advantage of correctly predicting the intrinsic mobility for organic materials. This is both useful for molecular design and for fundamental understandings of transport mechanisms in organic systems.

II. METHODOLOGICAL APPROACH

In classical Marcus theory, charge transport is modeled as sequential motion over barriers, with a rate that is proportional to $e^{-\Delta/kT}/\sqrt{T}$, where $\Delta = \lambda/4$ is the barrier height and λ
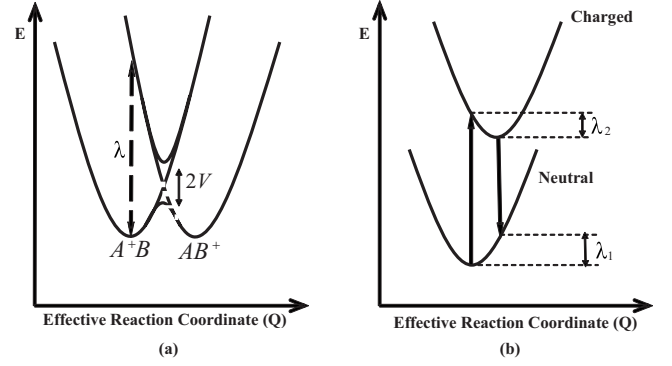
FIG. 2. Schemes related to hole transfer processes. (a) The reaction pathway for charge exchange due to transfer of a hole from molecule A to molecule B over a barrier within the harmonic oscillator approximation. (b) The reorganization energies for neutral and cationic molecules.

is the total reorganization energy (see Fig. 2). For the CT processes in a molecular dimer, A and B, the initial state is represented as $|A^+B\rangle$, and the final state is represented as $|AB^+\rangle$.

A. Quantum charge-transfer rate

The general quantum-mechanical CT rate was derived by Jortner[26] and Lin *et al.*[27] It starts with the Fermi golden rule,

$$k_{CT} = \frac{2\pi}{\hbar^2}|V|^2 \sum_v \sum_{v'} P_{iv} |\langle \Theta_{fv'}|\Theta_{iv}\rangle|^2 \delta(\omega_{fv',iv}), \quad (1)$$

where V is the electronic coupling (or transfer integral) between initial and final states, $\Theta_{i(f)}$ is the nuclear vibration wave function of the initial (final) states, consisting of product of (independent) harmonic oscillators, $\Theta_{iv} = \prod_j \chi_{iv_j}(Q_j)$ and $\Theta_{fv'} = \prod_j \chi_{fv'_j}(Q'_j)$, (see Fig. 2) where the wave function of a harmonic oscillator is

$$\chi_{v_j}(Q_j) = (\beta_j/\sqrt{\pi}2^{v_j}v_j!)^{1/2} H_{v_j}(\beta_j Q_j)\exp(-\beta_j^2 Q_j^2/2). \quad (2)$$

Here, $\beta_j = (\omega_j/\hbar)^{1/2}$ and H_{v_j} are the Hermite polynomials. P_{iv} is the distribution function for the collection of quanta $\{v_j\}$ of the initial state and is given by

$$P_{iv} = \left[\sum_v \exp\left(\frac{-E_{iv}}{k_B T}\right)\right]^{-1} \exp\left(\frac{-E_{iv}}{k_B T}\right)$$

$$= \prod_j 2 \sinh\frac{\hbar\omega_j}{2k_B T}\exp\left[\frac{-\hbar\omega_j\left(v_j + \frac{1}{2}\right)}{k_B T}\right]. \quad (3)$$

By redefining $P_{iv} = \prod_j P_{iv_j}$ and expressing the δ function as a Fourier integral in time, Eq. (1) may be recast as

$$k_{CT} = \frac{1}{\hbar^2}|V|^2 \sum_{v_1,v_2\cdots} \sum_{v_1',v_2'\cdots} \int_{-\infty}^{\infty} dt\, e^{it\omega_{fi}} \prod_j P_{iv_j} |\langle \chi_{fv_j'} | \chi_{iv_j}\rangle|^2$$

$$\times \exp\left\{ it\left[\left(v_j' + \frac{1}{2}\right)\omega_j' - \left(v_j + \frac{1}{2}\right)\omega_j\right]\right\}$$

$$= \frac{1}{\hbar^2}|V|^2 \int_{-\infty}^{\infty} dt\, e^{it\omega_{fi}} \prod_j G_j(t), \qquad (4)$$

where G_j is

$$G_j(t) = \sum_{v_j}\sum_{v_j'} P_{iv_j}|\langle \chi_{fv_j'}|\chi_{iv_j}\rangle|^2$$

$$\times \exp\left\{ it\left[\left(v_j' + \frac{1}{2}\right)\omega_j' - \left(v_j + \frac{1}{2}\right)\omega_j\right]\right\}. \qquad (5)$$

To evaluate G_j, the Slater sum (Mehler's formula) is employed:

$$\sum_{n=0}^{\infty} \frac{\exp\left[-\left(n+\frac{1}{2}\right)t\right]}{\sqrt{\pi}2^n n!} H_n(x)H_n(x')\exp\left[-\frac{1}{2}(x^2 + x'^2)\right]$$

$$= (2\pi \sinh t)^{-1/2}\exp\left[-\frac{1}{4}(x+x')^2\tanh\frac{1}{2}t\right.$$

$$\left. -\frac{1}{4}(x-x')^2\coth\frac{1}{2}t\right], \qquad (6)$$

where $H_n(x)$ are the Hermite polynomials. By the use of the vibrational wave functions [Eq. (2)], it is easily seen that

$$G_j = \frac{2\beta_j\beta_j' \sinh(\hbar\omega_j/2kT)}{2\pi(\sinh\kappa_j \sinh\mu_j')^{1/2}} \int dQ_j' dQ_j' dQ_j dQ_j$$

$$\times \exp\left\{-\frac{1}{4}\beta_j'^2\left[(Q_j' + Q_j')^2\tanh\frac{1}{2}\mu_j'\right.\right.$$

$$\left.\left. + (Q_j' - Q_j')^2\coth\frac{1}{2}\mu_j'\right]\right\}$$

$$\times \exp\left\{-\frac{1}{4}\beta_j^2\left[(Q_j + Q_j)^2\tanh\frac{1}{2}\kappa_j\right.\right.$$

$$\left.\left. + (Q_j - Q_j)^2\coth\frac{1}{2}\kappa_j\right]\right\}. \qquad (7)$$

Here, $\mu_j = -i\omega_j t$ and $\kappa_j = i\omega_j t + (\hbar\omega_j/kT)$ have been used. Under the displaced harmonic oscillator approximation, $\Delta Q_j = Q_j' - Q_j$ and $\omega_j = \omega_j'$, Eq. (7) becomes

$$G_j = \exp\left\{-S_j\left[\coth\left(\frac{\hbar\omega_j}{2kT}\right)\right.\right.$$

$$\left.\left. - \csc h\left(\frac{\hbar\omega_j}{2kT}\right)\cosh\left(i\omega_j t + \frac{\hbar\omega_j}{2kT}\right)\right]\right\}, \qquad (8)$$

where $\coth(x) = \frac{e^x + e^{-x}}{e^x - e^{-x}}$ and $\csc h(x) = \frac{2}{e^x - e^{-x}}$ are used. This can be further simplified using the phonon occupation number,

$$G_j = \exp\{-S_j[(1+2\bar{n}_j) - e^{i\omega_j t}(1+\bar{n}_j) - e^{-i\omega_j t}\bar{n}_j]\}. \qquad (9)$$

Here, $\bar{n}_j = \frac{1}{e^{\hbar\omega_j/k_B T}-1}$ denotes the population of the jth normal mode and ω_j is its frequency. $S_j = \lambda_j/\hbar\omega_j = \frac{1}{2}\hbar^{-1}\omega_j(\Delta Q_j)^2$ is the Huang-Rhys factor measuring the charge-phonon coupling strength and λ_j is the reorganization energy of the jth mode. Finally, the quantum CT rate is expressed as

$$k_{CT} = \frac{1}{\hbar^2}|V|^2 \int_{-\infty}^{\infty} dt\, \exp\left\{ i\omega_{fi}t - \sum_j S_j[(2\bar{n}_j + 1) - \bar{n}_j e^{-i\omega_j t}\right.$$

$$\left. - (\bar{n}_j + 1)e^{i\omega_j t}]\right\}. \qquad (10)$$

The above equation is given by Lin *et al.*[27] for a general nonradiative transition process for two-level system. For our case, $\omega_{fi} = 0$. Equation (10) is a full quantum expression in perturbation theory which considers all the vibrational modes at quantum-mechanical level. As far as we know, this formula has never been used in organic materials. In the strong-coupling $(\Sigma_j S_j \gg 1)$ and high-temperature limits $(\hbar\omega_j/kT \ll 1, \bar{n}_j \approx k_B T/\hbar\omega_j,$ and the classical limit), the short-time approximation can be applied, in which case it can be shown that Eq. (10) goes to the Marcus formula:[8]

$$k_{CT} = \frac{|V|^2}{\hbar}\left(\frac{\pi}{\lambda k_B T}\right)^{1/2}\exp\left(-\frac{\lambda}{4k_B T}\right), \qquad (11)$$

with $\lambda = \Sigma_j \lambda_j = \Sigma_j S_j \hbar\omega_j$. Although it has been broadly used to investigate the charge transport in organic semiconductors,[9–14] the nuclear vibrational effect is completely neglected.

B. Calculation of transfer integral

We use the crystal structures of Fig. 1 to generate all the possible nearest-neighbor intermolecular hopping pathways for hole transport. For a given transport pathway, the transfer integral can be calculated in diabatic representation. The initial state ($|D^+A\rangle$) and final state ($|DA^+\rangle$) during the CT process correspond to two diabatic states that the hole localizes on the donor and acceptor molecules, respectively. Then, the transfer integral is written as

$$V = \langle D^+A|H_{DA}|DA^+\rangle, \qquad (12)$$

where H_{DA} is the interaction Hamiltonian between donor and acceptor. The transfer integral can be obtained either by Koopmans' theorem or by directly evaluating the electronic coupling element for frontier orbitals.

Based on Koopmans' theorem, the transfer integral is equal to the energy splitting between the highest occupied molecular orbital (HOMO) and HOMO-1 of the dimer.[28] However, Valeev *et al.*[29] noticed that when the dimer is not cofacially stacked, the site-energy correction due to the crystal environment should be taken into account.

In modeling scanning tunneling microscopy, Fujita *et al.*[30] worked out a direct scheme to obtain the transfer integral. At the Hartree-Fock (HF) level, the transfer integral can be written as

$$V = \langle \phi_{\mathrm{HOMO}}^{0,\mathrm{site1}} | F^0 | \phi_{\mathrm{HOMO}}^{0,\mathrm{site2}} \rangle, \qquad (13)$$

where $|\phi_{\mathrm{HOMO}}^{0,\mathrm{site1}}\rangle$ and $|\phi_{\mathrm{HOMO}}^{0,\mathrm{site2}}\rangle$ represent the HOMOs of the two adjacent molecules, 1 and 2, when no intermolecular interaction is presented. F^0 is the Fock operator for the dimer, and the suffix zero indicates that the molecular orbitals appearing in the operator are unperturbed. However, it has been shown that the HF bandwidth (closely related to the transfer integral) for a polymer is always about 20%–30% larger than the result from (photoemission) experiments.[31] Moreover the electronic coupling from the density-functional theory (DFT) orbital is usually about 20% less than that from HF.[32] Therefore, we use the Kohn-Fock operator instead of the Fock operator to obtain the transfer integral in the framework of the DFT. Here, the Kohn-Fock operator is

$$F^0 = SC\varepsilon C^{-1}, \qquad (14)$$

where S is the intermolecular overlap matrix, and C and ε are the dimer Kohn-Sham orbital's coefficients and energies. The noninteracting molecular orbitals of the two individual molecules are calculated separately by the standard self-consistent field procedure. These noninteracting orbitals are then used to construct the dimer Kohn-Fock matrix. Namely, it takes directly the unperturbed individual molecule's orbital and density matrix to guarantee that originally, the two molecules are noninteracting, and only when putting them together, one can get interaction information with respect to the individual molecules in the spirit of first-order perturbation. All of the calculations are performed with the GAUSSIAN 03 package.[33] The PW91 exchange and PW91 correlation functionals plus a 6-31G* basis set are employed, which has been shown to give the best description for electronic couplings at the DFT level.[34] This direct method was widely used by Troisi *et al.*[24,25,35] in studying pentacene, DNA, and rubrene, by Senthikumar *et al.*,[36] and by our group in our previous work.[13–15] There are other methods for transfer integrals, such as site-energy correction method[29] and minimal energy splitting method.[37] Our recent calculation has proved that all these three approaches are almost equivalent in determining the transfer integrals of pentacene dimers with different tilt angles.[38]

C. Random-walk simulations for mobility

Given the quantum CT rates, the charge mobility may be obtained by assuming a diffusion process and using the Einstein formula $\mu = \frac{eD}{k_B T}$. The isotropic charge diffusion constant D is simulated by a random walk through the molecular crystal structure (see Fig. 1). We choose one molecule as the initial charge center. The charge hops between nearest-neighbor molecules with a probability $p_\alpha = \frac{k_{CT}^\alpha}{\sum_\alpha k_{CT}^\alpha}$ for the αth pathway, with the summation in the denominator running over all the pathways in 3D. The hopping time is $1/k_{CT}^\alpha$ and the hopping distance is taken to be the molecular center-center distance. At each step, a random number r uniformly distributed between 0 and 1, is generated. If $\sum_{\alpha=1}^{j-1} p_\alpha < r \leq \sum_{\alpha=1}^{j} p_\alpha$, then the charge is assumed to move along the jth direction. We save the squared displacement every 100 ns, which is much larger than the time cost in the transfer be-
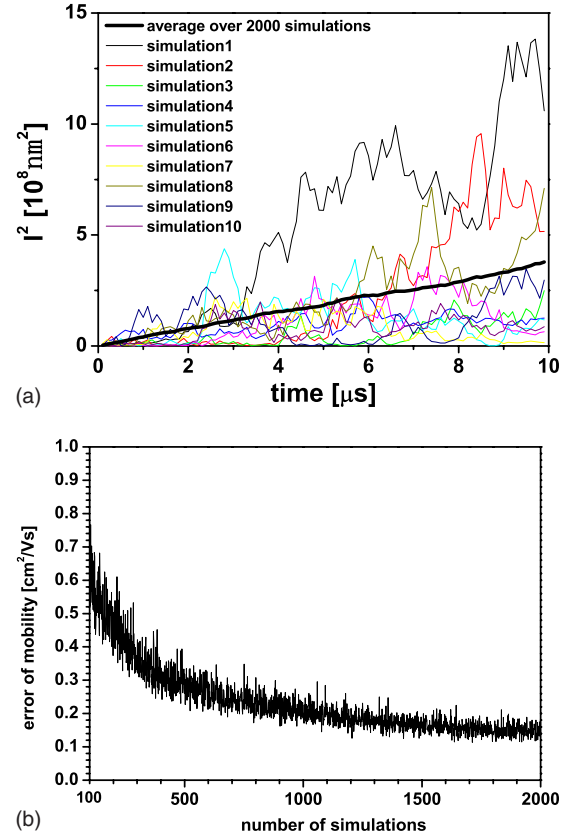
FIG. 3. (Color online) (a) Squared displacement versus simulation time for rubrene. Each thin solid line represents the individual simulation. The thick solid line means the average over 2000 simulations. (b) The error in estimating the mobility vs the number of simulations for rubrene.

tween the neighbors. The time for each random walk is chosen to be 10 μs, which is again much larger than the time of the snapshot. The displacement between the initial and final points is then evaluated. In order to obtain a converged diffusion constant, as indicated by a linear relationship between the square of the diffusion distance and the diffusion time, a few thousand times of simulation are performed. The diffusion constant is then obtained as $D = \lim_{t\to\infty} l(t)^2/6t$, where $l(t)^2$ is the mean-squared displacement. In this paper, 2000 simulations have been performed to get a converged mobility. In Fig. 3(a), we plot the results of ten simulations as well as the average of 2000 samples for rubrene. It should be mentioned that such simulation actually gives the 3D averaged mobility although our calculations are based on the structure of single crystals.

To achieve the statistical error of the diffusion constant, one would sort to carry out many times such process, each of which contains 2000 simulations, but this would be much time consuming. Thus, we adopt a simpler sampling approach. We suppose that the 2000 simulations for mobility are large enough. Each simulation result is regarded as a point. We randomly select one point out of the 2000 points for 2000 times. Then we can have another set of 2000 points. It should be noted that the same point could be selected several times because each selection is independent. We do such random process for 100 times and calculate the mobili-

ties $\{\mu_i\}$ separately. The error of the diffusion constant simulation is evaluated by $\frac{1}{2}\max\{\mu_i\}-\frac{1}{2}\min\{\mu_i\}$. Figure 3(b) shows the error of the mobility as a function of the number of samplings. We can see clearly that the error of the mobility depends on the used samples and come to converge when the number of the sampling is larger than 1500. This proves that our 2000 samples are enough to cover the whole sample space.

Note that organic crystals typically have layered structures with weak couplings between layers. Thus, the isotropic diffusion assumed previously[11–13] is not valid where $D = \frac{1}{2d}\Sigma_i r_i^2 k_i P_i$ has been used and the details for the symbols can be seen there. The present approach works well for general 3D anisotropic cases and is equivalent to the above isotropic diffusion when all the directions are isotropic. We have also carried out simulations for a pure two-dimensional (2D) layer, and comparison between 2D and 3D will be discussed later. The simulation results should be close to measurements done on a well-ordered solid film since the random-walk simulation represents a spatial average. Defects, microcrystalline boundaries, as well as film morphology, are neglected at this stage. We are currently extending the present approach to include such effects.

III. RESULTS AND DISCUSSION

The information of all the vibrational modes such as frequencies and reorganization energies are required in Eq. (10). The total reorganization energy λ includes the molecular geometry modifications that occur when a charge is added or removed from a molecule (inner reorganization) as well as the modifications in the surrounding medium due to polarization effects (outer reorganization). Here, we focus on the inner reorganization energy that reflects the geometry relaxation energies of one molecule (which accepts the hole) going from the neutral-state geometry to the positively charged-state geometry and an adjacent molecule (which donates the hole) evolving in the opposite way (see Fig. 2). The λ terms were evaluated in two ways: (i) they were computed directly from the adiabatic potential-energy surfaces of neutral and charged species; (ii) they were obtained on the basis of a normal-mode (NM) analysis, which divides the total relaxation energy into the contribution from each vibrational mode.

The geometries of the neutral and charged species were optimized at the DFT level with the hybrid B3LYP functional and 6-31G** basis set, and the vibrational frequencies and NMs were evaluated. The reorganization energy and Huang-Rhys factor of each NM can then be obtained through the DUSHIN program developed by Reimers.[39] The total reorganization energies obtained from the adiabatic potential approach ($\lambda=\lambda_1+\lambda_2$ in Fig. 2) are 150 and 105 meV for rubrene and tetracene, respectively, in good agreement with previous calculations.[21] These values are very close to those obtained by summing the reorganization energies from the individual normal modes, 150 and 109 meV, respectively. This agreement indicates that the harmonic oscillator approximation provides an excellent description of the CT process for the present molecules. The reorganization energies
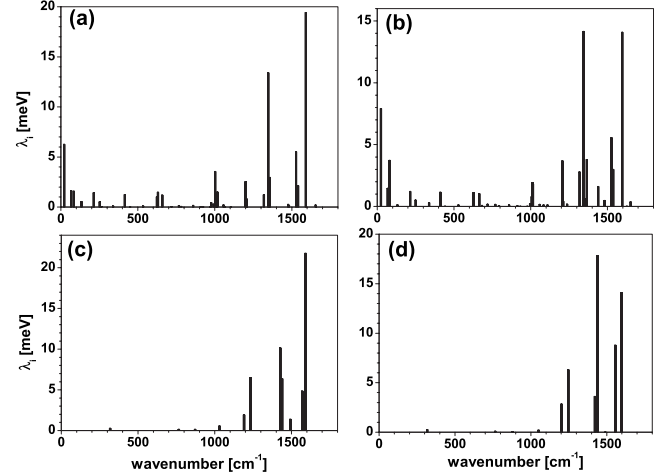
FIG. 4. Contribution of the individual vibrational modes to the relaxation energies for neutral ($\lambda_i^{(1)}$) and cationic ($\lambda_i^{(2)}$) molecules of rubrene and tetracene; (a) neutral rubrene; (b) cationic rubrene; (c) neutral tetracene; and (d) cationic tetracene.

for each normal mode are presented in Fig. 4. Rubrene differs from tetracene in the low-frequency region due to the twisting motions of the four phenyl groups being strongly coupled with the CT process. We also see that for both molecules, the high-frequency modes (C-C bond-stretching) present dominant electron-phonon couplings, and it will be shown below that these couplings lead to the bandlike behavior for the mobility.

From Eqs. (13) and (14), we can obtain the transfer integral along any direction in the crystals. Our calculation shows that the largest transfer integral for rubrene comes from the a direction (102.4 meV) which is larger than that for tetracene and pentacene, respectively. This can be understood from the molecular packing. Both rubrene and tetracene (or pentacene) have a herringbone motif in the ab plane where the most significant electronic couplings are found. However, the modulation of the phenyl side groups in rubrene makes the long molecule axes lie in the ab plane in rubrene, while in tetracene (or pentacene), they come out of that plane. This modulation leads to no short-axis displacement along the a direction and cofacial π-stack with some long-axis displacement. Although such long-axis sliding goes against the electronic coupling between adjacent molecules, Brédas *et al.*[21] showed at the INDO level that the sliding happens to the place where the interaction between the π-atomic orbitals constructively reaches a maximum and results much larger electronic coupling along a direction than along b direction. This is consistent with our calculation for rubrene.

The CT rates for all dimers are numerically calculated through Eq. (10). For computational convenience, we can rewrite Eq. (10) as

$$k_{CT} = \frac{2}{\hbar^2}|V|^2 \int_0^\infty dt \, \exp\left[-\sum_j S_j(2\bar{n}_j+1)(1-\cos\omega_j t)\right]$$
$$\times \cos\left(\sum_j S_j \sin \omega_j t\right). \tag{15}$$
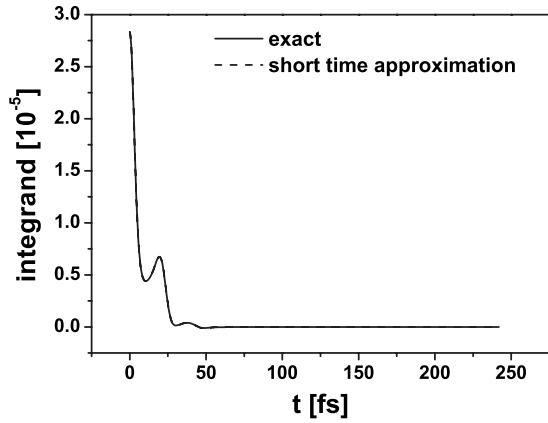
FIG. 5. The integrand of Eq. (13) as a function of time at 300 K for rubrene. Solid line is the exact result from Eq. (13). Dash line is the result from the short-time approximation. It is difficult to distinguish them, indicating short-time approximation is reasonable.

For rubrene, the integrand of Eq. (15) decays quickly with time, see Fig. 5, where the integrand goes to zero when the time reaches 100 fs. It is thus enough to use 0–150 fs as the integration region. The Simpson integration method is applied to calculate Eq. (15) with the integral region being divided into 500 intervals. However, convergence problems may arise in the time integration of Eq. (15), as occurred in the case of tetracene. The integrand oscillates with time and does not show any decay. We therefore apply a short-time approximation for the mode that possesses the most significant Huang-Rhys factor:

$$e^{i\omega_j t} \approx 1 + i\omega_j t + \frac{1}{2}(i\omega_j t)^2, \qquad (16)$$

where the last term provides an overall decay factor of $e^{-\omega_j^2 t^2/2}$ in the integrand and guarantees the convergence. For tetracene, the mode with the largest Huang-Rhys factor (S_1 =0.11) is that with ω_j=1592 cm^{-1}. We have verified that even in the case of rubrene, where Eq. (15) can be easily integrated without approximation, the short-time approximation works well if the mode with strongest electron-phonon coupling is selected (see Fig. 5).

Figure 6(a) shows the temperature-dependent CT rate of the most closely packed dimer along a direction in the rubrene single crystal. The transfer rate becomes independent of temperature below 5 K (see the inset), as expected for nuclear tunneling. It then increases with temperature and reaches a maximum at about 130 K and finally starts to decrease. From the mobility curve of Fig. 6(b), it is seen that, overall, the mobility behaves bandlike (decreasing with temperature). Meanwhile, there are some fine features at low temperatures. The mobility decreases rapidly from 1 to 10 K and then increases slowly with temperature until 30 K, and when above 30 K, it decreases again. These can be fully justified by the general k_{CT}/T behavior. At very low temperature, the CT rate is independent of temperature, so the mobility decreases as $1/T$. Then, the CT rate enters a region corresponding to thermal activation over a barrier. In
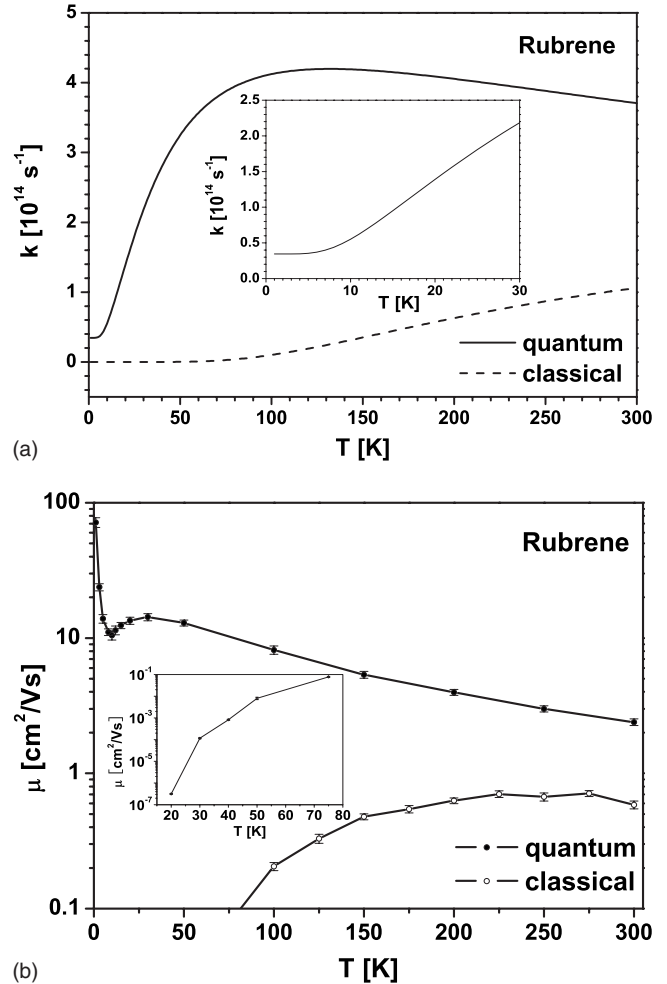
FIG. 6. (a) Hole transfer rates (k's) as a function of temperature for the rubrene dimer with the largest electronic coupling. The classical Marcus theory and the present quantum theory are compared. The inset is to show more clearly that the transfer rate from the present theory is almost constant below 5 K; (b) 3D averaged hole mobilities (μ's) as a function of temperature in rubrene obtained from the present quantum theory and Marcus theory. The inset shows the mobility from Marcus theory in low temperatures.

classical Marcus theory, the barrier height is $\frac{\lambda}{4}$=150/4 =37.5 meV$\approx$435 K. The nuclear vibrational effect reduces this height to only 130 K. Thus, when $T > 130$ K, the barrier is fully overcome and the carrier behaves like a bandlike hole.

For tetracene, see Fig. 7, both k_{CT} and μ differ considerably from those of rubrene. Up to 70 K, k_{CT} remains constant due to nuclear tunneling and then starts to decrease. The bandlike behavior for mobility is seen for the whole range of temperature. We conclude that for tetracene, or similarly other polyacene, the hopping character should not be observed because the vibrational modes that are strongly coupled with hole motion are of high frequency. These crystals mainly exhibit bandlike behaviors due to the nuclear tunneling associated with high-frequency modes.

At this stage, some notes should be given. The present mobility reflects the averaged diffusion ability for 3D space,
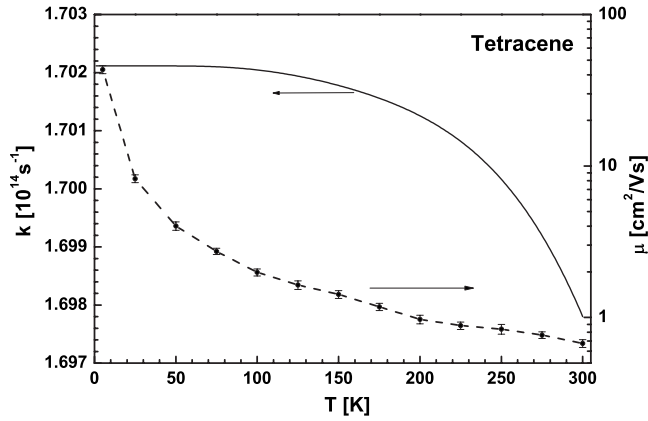
FIG. 7. Hole transfer rate (k) and 3D averaged hole mobility (μ) in tetracene as a function of temperature obtained from the present quantum theory. The hole transfer rate is obtained from the tetracene dimer with the largest electronic coupling.

TABLE I. Random-walk simulated room-temperature hole mobility (in $cm^2/V\,s$) based on the quantum transfer rate for a 3D lattice and a a-b plane layered 2D structure.

	Pentacene	Rubrene	Tetracene
3D	2.01 ± 0.10	2.39 ± 0.14	0.67 ± 0.04
2D	4.77 ± 0.23	6.67 ± 0.44	1.68 ± 0.08

but the molecular crystal is usually anisotropic. Thus, the direct comparison between our data and the experiment measurements along each direction is not reasonable. Since only intramolecular modes are considered here, the mobility versus temperature behavior along each direction is the same as the 3D random-walk simulation which is decided by the integrand of Eq. (10). The experimental measurements indeed demonstrated that mobility versus temperature behavior is the same for a and b directions.[16,20] It can be seen that our predicted mobility versus temperature behavior is consistently close to that from 175 to 300 K (Refs. [16] and [20]) and is still reasonable in lower-temperature region.[19] We also note that such bandlike behaviors over the whole range of temperature have been evidenced clearly in experiments for naphthalene and anthracene single crystals[18] and for tetracene single crystal.[40] Meanwhile, the calculations for naphthalene with Hostein-Peierls model further show that the dependence of the mobility on temperature is almost the same along different directions for hole transport where intermolecular modes have been included.[6,7] As analyzed above, intramolecular modes exhibit bandlike behavior; it seems that the intermolecular vibrations can contribute similar mobility versus temperature relation to intramolecular vibrations in naphthalene for hole transport. Because the mobility sensitively depends on molecular packing,[7,41,42] whether it is such case for rubrene and tetracene, it needs to be further investigated. Despite of the 3D average, the present calculation can also predict the transport ability for each system reasonably. For example, the room-temperature mobility is calculated to be 2.4 $cm^2/V\,s$ for rubrene and 0.67 $cm^2/V\,s$ for tetracene. Note that our calculation for pentacene at the same level gives a value of 2.0 $cm^2/V\,s$ for the room-temperature hole mobility, which is smaller than the value of rubrene even though the reorganization energy of rubrene (150 meV) is much larger than that of pentacene (92 meV). This is consistent with the experiments.[43] Our previous calculation for thiophenes also shows that such average can give reasonable prediction for charge transport.[15]

We next compare 3D and 2D simulations to reveal the anisotropic behavior of the transport. In fact, in organic field effect transistor devices, it has often been assumed that only a single or very few molecular layers close to the organic/insulator interface participate in electrical conduction because of the transverse modulation by the gate bias. In an extremely ideal case, the a-b plane of the herringbone structure is parallel to the (perfect) interface. Then a 2D simulation will give an estimate on how the mobility anisotropy behaves. We list the room-temperature hole mobility for pentacene, rubrene, and tetracene in Table I. It is seen that due to the weak interlayer coupling, the mobility is reduced by about a factor of 2.3–2.8 from 2D to 3D structures. As far as we know, the mobility of thin films for pentacene and rubrene can reach 1.5 (Ref. [44]) and 0.7 $cm^2/V\,s$,[45] respectively. Since grain boundaries and interfacial disorder inevitably exist in thin films and limit the charge transport, it is not ready for a detailed comparison between measured and calculated data.

Finally, we should point out some limitations of the present approach. A number of approximations have been made regarding the hopping mechanism: (i) temperature-independent electronic coupling V is assumed although V is subject to thermal fluctuation as pointed out by Troisi;[23–25] (ii) the simple dimer model has neglected the external polarization and the contribution of surrounding molecules to the reorganization; and (iii) strong dissipation is assumed to validate the hopping mechanism, which completely ignores the quantum recrossing (coherent) events. (The intermolecular electronic couplings are large enough to cause such coherent effects, and here only quantum nuclear tunneling is considered in the hopping framework.) As pointed out earlier, a first-principles quantum coherent model such as the Holstein-Peierls model overestimates the mobility by 2 orders of magnitude.[7] Fluctuations certainly lead to a localized charge description which, to some extent, conforms to the hopping model. The intermolecular vibrations are important for charge transport. For instance, the coupling of the CT process with the low-frequency modes in the surrounding medium would introduce a friction to the charge motion and eventually reduce the mobility. How the intermolecular modes affect the mobility versus temperature behavior is difficult to answer and consists of great challenges in such complex systems as organic semiconductors. There is clearly still considerable work needed to obtain a complete description of charge transport in soft organic materials. Nevertheless, the present approach does contain some essential features regarding charge transport in organic materials, which is embodied not only in reasonable temperature dependence but also in quantitative description of the room-temperature mobility.[5–7,11–15,23,25,46–49]

IV. CONCLUSION

To conclude, a quantum-mechanical CT approach that couples first-principles DFT calculations with a random-walk simulation was used to study the temperature dependence of the 3D averaged hole mobility of rubrene and tetracene. Meanwhile, the average mobility in the 2D simulation is used as a rough estimation of the mobility in thin films due to the isotropic transport property. Nuclear tunneling effects are found to be very important in understanding the carrier transport in these organic materials. Bandlike behaviors are obtained for a wide range of temperature in both systems.

The room-temperature mobility and the bandlike behaviors predicted by our approach are both in good agreement with recent experiments.

*zgshuai@iccas.ac.cn

[1] V. Coropceanu, J. Cornil, D. A. da Silva Filho, Y. Olivier, R. Silbey, and J. L. Brédas, Chem. Rev. (Washington, D.C.) **107**, 926 (2007).

[2] M. E. Gershenson, V. Podzorov, and A. F. Morpurgo, Rev. Mod. Phys. **78**, 973 (2006).

[3] A. Facchetti, Mater. Today **10**, 28 (2007).

[4] V. C. Sundar, J. Zaumseil, V. Podzorov, E. Menard, R. L. Willett, T. Someya, M. E. Gershenson, and J. A. Rogers, Science **303**, 1644 (2004).

[5] K. Hannewald and P. A. Bobbert, Phys. Rev. B **69**, 075212 (2004).

[6] K. Hannewald and P. A. Bobbert, Appl. Phys. Lett. **85**, 1535 (2004).

[7] L. J. Wang, Q. Peng, Q. K. Li, and Z. Shuai, J. Chem. Phys. **127**, 044506 (2007); L. J. Wang, Q. K. Li, and Z. Shuai, *ibid.* **128**, 194706 (2008).

[8] R. A. Marcus, Rev. Mod. Phys. **65**, 599 (1993).

[9] J. L. Brédas, J. P. Calbert, D. A. da Silva Filho, and J. Cornil, Proc. Natl. Acad. Sci. U.S.A. **99**, 5804 (2002).

[10] Y. A. Berlin, G. R. Hutchison, P. Rempala, M. A. Ratner, and J. Michl, J. Phys. Chem. A **107**, 3970 (2003); G. R. Hutchison, M. A. Ratner, and T. J. Marks, J. Am. Chem. Soc. **127**, 16866 (2005).

[11] W. Q. Deng and W. A. Goddard III, J. Phys. Chem. B **108**, 8614 (2004).

[12] Y. B. Song, C. A. Di, X. D. Yang, S. P. Li, W. Xu, Y. Q. Liu, L. M. Yang, Z. G. Shuai, D. Q. Zhang, and D. B. Zhu, J. Am. Chem. Soc. **128**, 15940 (2006).

[13] X. D. Yang, Q. K. Li, and Z. Shuai, Nanotechnology **18**, 424029 (2007).

[14] S. W. Yin, Y. P. Yi, Q. X. Li, G. Yu, Y. Q. Liu, and Z. G. Shuai, J. Phys. Chem. A **110**, 7138 (2006).

[15] X. D. Yang, L. J. Wang, C. L. Wang, W. Long, and Z. G. Shuai, Chem. Mater. **20**, 3205 (2008); C. L. Wang, F. H. Wang, X. D. Yang, Q. K. Li, and Z. G. Shuai, Org. Electron. **9**, 635 (2008).

[16] V. Podzorov, E. Menard, A. Borissov, V. Kiryukhin, J. A. Rogers, and M. E. Gershenson, Phys. Rev. Lett. **93**, 086602 (2004).

[17] O. D. Jurchescu, J. Baas, and T. T. M. Palstra, Appl. Phys. Lett. **84**, 3061 (2004).

[18] N. Karl, Synth. Met. **133-134**, 649 (2003).

[19] O. Ostroverkhova, D. G. Kooke, F. A. Hegmann, J. E. Anthony, V. Podzorov, M. E. Gershenson, O. D. Jurchescu, and T. T. M.

Palstra, Appl. Phys. Lett. **88**, 162101 (2006).

[20] V. Podzorov, E. Menard, J. A. Rogers, and M. E. Gershenson, Phys. Rev. Lett. **95**, 226601 (2005).

[21] D. A. da Silva Filho, E. G. Kim, and J. L. Brédas, Adv. Mater. **17**, 1072 (2005).

[22] J. R. Weinberg-Wolf, L. E. McNeil, S. B. Liu, and C. Kloc, J. Phys.: Condens. Matter **19**, 276204 (2007).

[23] A. Troisi and G. Orlandi, Phys. Rev. Lett. **96**, 086601 (2006).

[24] A. Troisi and G. Orlandi, J. Phys. Chem. A **110**, 4065 (2006).

[25] A. Troisi, Adv. Mater. **19**, 2000 (2007).

[26] J. Jortner, J. Chem. Phys. **64**, 4860 (1976).

[27] S. H. Lin, C. H. Chang, K. K. Liang, R. Chang, Y. J. Shiu, J. M. Zhang, T. S. Yang, M. Hayashi, and F. C. Hsu, Adv. Chem. Phys. **121**, 1 (2002).

[28] B. C. Lin, C. P. Cheng, Z. Q. You, and C. P. Hsu, J. Am. Chem. Soc. **127**, 66 (2005).

[29] E. F. Valeev, V. Coropceanu, D. A. da Silva Filho, S. Salman, and J. L. Brédas, J. Am. Chem. Soc. **128**, 9882 (2006).

[30] T. Fujita, H. Nakai, and H. Nakatsuji, J. Chem. Phys. **104**, 2410 (1996).

[31] J. M. André, J. Delhalle, and J. L. Brédas, *Quantum Chemistry Aided Design of Organic Polymers: An Introduction to the Quantum Chemistry of Polymers and its Applications* (World Scientific, Singapore, 1991).

[32] C. J. Calzado and J. P. Malrieu, Chem. Phys. Lett. **317**, 404 (2000).

[33] M. J. Frisch *et al.*, GAUSSIAN 03, revision A. 1, Gaussian, Inc., Pittsburgh PA, 2003.

[34] J. S. Huang and M. Kertesz, Chem. Phys. Lett. **390**, 110 (2004).

[35] A. Troisi and G. Orlandi, Chem. Phys. Lett. **344**, 509 (2001).

[36] K. Senthilkumar, F. C. Grozema, F. M. Bickelhaupt, and L. D. A. Siebbeles, J. Chem. Phys. **119**, 9809 (2003).

[37] X. Y. Li, J. Comput. Chem. **22**, 565 (2001).

[38] G. J. Nan, L. J. Wang, X. D. Yang, Z. G. Shuai, and Y. Zhao, J. Chem. Phys. **130**, 024704 (2009).

[39] J. R. Reimers, J. Chem. Phys. **115**, 9103 (2001).

[40] R. W. I. de Boer, M. Jochemsen, T. M. Klapwijk, and A. F. Morpurgo, J. Appl. Phys. **95**, 1196 (2004).

[41] Z. Rang, A. Haraldsson, D. M. Kim, P. P. Ruden, M. I. Nathan, R. J. Chesterfield, and C. D. Frisbie, Appl. Phys. Lett. **79**, 2731 (2001).

[42] Z. Rang, M. I. Nathan, P. P. Ruden, V. Podzorov, M. E. Gershenson, C. R. Newman, and C. D. Frisbie, Appl. Phys. Lett. **86**,

123501 (2005).

[43] C. Goldmann, S. Haas, C. Krellner, K. P. Pernstich, D. J. Gundlach, and B. Batlogg, J. Appl. Phys. **96**, 2080 (2004).

[44] S. F. Nelson, Y.-Y. Lin, D. J. Gundlach, and T. N. Jackson, Appl. Phys. Lett. **72**, 1854 (1998).

[45] N. Stingelin-Stutzmann, E. Smits, H. Wondergem, C. Tanase, P. Blom, P. Smith, and D. de Leeuw, Nature Mater. **4**, 601 (2005).

[46] R. W. Munn and R. Silbey, J. Chem. Phys. **83**, 1843 (1985).

[47] R. W. Munn and R. Silbey, J. Chem. Phys. **83**, 1854 (1985).

[48] V. M. Kenkre, J. D. Andersen, D. H. Dunlap, and C. B. Duke, Phys. Rev. Lett. **62**, 1165 (1989).

[49] Y. C. Cheng and R. J. Silbey, J. Chem. Phys. **128**, 114713 (2008).